applied sciences

MDPI

Article

A Study on Paste Flow and Pipe Wear in Cemented Paste Backfill Pipelines

Xiangyu Xie [1], Scott Cheevers [2], Y. X. Zhang [1,3,*], Kejun Dong [1], Zhongpu (Leo) Zhang [1], Dean Harty [2], Andrew Stonier-Gibson [2] and Richard (Chunhui) Yang [1,*]

[1] Centre for Advanced Manufacturing Technology, School of Engineering, Faculty of Engineering, Computing and Science, Western Sydney University, Locked Bag 1797, Penrith, NSW 2751, Australia
[2] Metrologi Pty Ltd., P.O. Box 3331, Rouse Hill, NSW 2155, Australia
[3] School of Mechanical and Mechatronic Engineering, University of Technology Sydney, 81 Broadway, Ultimo, NSW 2007, Australia
* Correspondence: sarah.zhang@uts.edu.au (Y.X.Z.); r.yang@westernsydney.edu.au (R.Y.)

Featured Application

This study develops an advanced computational fluid dynamics (CFD)-based analysis framework to investigate flow dynamics of the CPB and the wear conditions of the pipeline, which considers the slip layer and shear-induced particle migration inside pipes. It provides a robust predictive tool for optimising CPB pipeline design and operating conditions in the mining industry.

Abstract

Cemented paste backfill (CPB) is widely used in mining operations to enhance underground stope stability, production, and safety. Accurately predicting paste flow behaviours in backfill reticulation circuits is crucial for efficient delivery control and asset longevity. However, the predictions remain challenging due to complex rheology and flow-induced particle heterogeneities of CPB. This study develops a computational fluid dynamics (CFD)-based analysis framework to investigate flow dynamics of the CPB and the wear conditions of the pipes, considering slip layer and shear-induced particle migration. Experimental loop tests are conducted to measure pressure drops of CPB at different velocities, providing data for validating the developed CFD model. Simulation results are in good agreement with the measured pressure drops and wear rates of the internal pipeline wall. Furthermore, comparisons with existing models indicate that the developed model provides more accurate predictions. Microscopical analyses reveal that shear-induced particle migration leads to the formation of a distinct plug flow region, with particles accumulating near the unyielded boundary. Meanwhile, a low particle concentration near the pipe wall reduces local viscosity and pressure drop. Parametric studies reveal that increased flow velocity and reduced pipe diameter significantly elevate both pressure drop and wear rate, while higher solid concentrations induce nonlinear rheological effects.

Keywords: cemented paste backfill (CPB); computational fluid dynamics (CFD); reticulation system; shear-induced particle migration; pressure drop analysis; pipe wear

Check for updates

Academic Editor: Alberto Benato

Received: 30 December 2025
Revised: 12 January 2026
Accepted: 20 January 2026
Published: 24 January 2026

Copyright: © 2026 by the authors. Licensee MDPI, Basel, Switzerland. This article is an open access article distributed under the terms and conditions of the Creative Commons Attribution (CC BY) license.

1. Introduction

Backfilling in underground mining involves filling excavated voids or stopes to enhance ground stability and minimise surface subsidence. It also mitigates environmental

risks by reducing land disturbance and preventing the spread of contaminants into surrounding ecosystems. Commonly used backfill materials include waste rocks, tailings, or cement-based binders, which provide mechanical support to surrounding rock masses. Efficient delivery of backfill to underground operations is facilitated through a system of reticulation circuits, transporting materials from surface processing facilities or storage locations to target areas [1]. The design of these delivery systems requires careful considerations of material properties, flow conditions, and operational efficiency to minimise costs, ensure safety, and support sustainable mining practices.

Effective management of the cemented paste backfill (CPB) flow in pipelines is the most critical concern, as it directly impacts the durability and efficiency of backfill delivery systems. CPB circuits often involve significant elevation changes. The CPB would descend at high velocity and affect the vertical casing intensively [1,2]. The abrasive components in CPB, such as fine particles, waste rock, or tailings, accelerate pipeline wear over time [3–6]. To mitigate this issue, operators adjust the head height of the pastefill line to minimise freefall and uncontrolled velocity while still generating a controlled vacuum at the borehole top to facilitate CPB intake when direct pumping is unavailable. Achieving this balance requires precise control of rheology, flow velocity, and pressure. Therefore, accurately predicting CPB flow behaviour and pipe wear conditions is essential for enhancing the safety, reliability, and operational efficiency of CPB delivery systems.

To efficiently estimate the CPB flow behaviours in pipelines, various empirical and analytical models have been developed in the literature [7–9]. These models rely heavily on the accurate measurement of key rheological parameters, such as viscosity and yield stress, which are typically obtained using a rotational viscometer. However, due to its complex composition, CPB exhibits different rheological behaviour when flowing through pipelines compared to when sheared in viscometers [10]. This often leads to significant deviations when viscometer-measured parameters are used to predict pipeline pressure drops [9]. Therefore, loop tests are commonly performed to directly measure rheological parameters under pipeline-like conditions, providing more accurate data for analytical models [8]. These tests typically involve a closed-circuit pipeline system equipped with pumps, flow meters, and pressure sensors to assess flow behaviour. Advanced loop system features industry-scale pipe diameters (exceeding 100 mm), slopes, and bends, which better simulate the real delivery conditions at mine sites [11]. However, loop tests are labour-intensive and require large quantities of raw materials, which significantly increases their complexity and cost.

In recent years, numerical modelling has been employed as a more efficient alternative to loop tests for predicting CPB flow behaviour [12,13]. However, the inherent complexity of CPB rheology presents significant challenges in achieving accurate predictions. To fulfil strength and load-bearing capacity requirements [14,15], CPB is typically formulated with a high solid mass concentration (exceeding 70%). This high concentration results in characteristic features of dense solid dispersions, such as high yield stress, shear-thinning, and thixotropy [16–18]. In some cases, plasticisers are added to ensure sufficient flowability without compromising the targeted cured strength, further complicating CPB's rheological properties. The rheological behaviour of CPB can be incorporated into numerical models by introducing rheological models to describe its shear response, such as the Herschel-Bulkley (H-B) and the thixotropic models [19]. Some advanced models also account for temperature-dependent rheology properties to achieve more accurate predictions [20]. These models allow for an accurate representation of the relationship between shear stress and shear rate, enabling the model to capture the complex flow behaviour of CPB under varying conditions.

A key limitation of existing models is the assumption that CPB behaves as a homogeneous medium during pipeline transport. In practice, the particle distribution and rheological properties of CPB within the pipe cross-section are highly heterogeneous. These heterogeneities arise from shear-induced particle migration and wall effects under confined flow conditions, which lead to non-uniform particle concentrations and spatially varying rheology. Shear-induced particle migration drives particles away from the pipe wall to the pipe centre [21,22], while the presence of the wall inhibits particle accumulation, leading to lower packing density near the wall compared to bulk material [23]. These factors contribute to the formation of a distinct slip layer at the interface between the pipe wall and the main CPB flow. Particle Image Velocimetry (PIV) measurements of CPB flow in transparent pipes revealed that the presence of a slip layer leads to an abrupt increase in flow velocity near the pipe wall [24]. Recent studies show that incorporating the wall slip effects into numerical models has significantly improved the accuracy of pressure drop predictions [25]. In addition to the slip layer, shear-induced particle migration also affects particle distribution within the bulk material, leading to variations in local rheology across the pipe cross-section [26]. These particle heterogeneities introduce additional complexity in modelling the flow behaviour of CPB, a challenge that has not yet been addressed thoroughly. Overcoming this requires the development of more robust numerical models that incorporate particulate flow dynamics and other complex interactions within CPB systems.

In this study, a novel advanced computational fluid dynamics (CFD)-based numerical analysis framework is developed to predict the flow behaviours of CPB in pipelines, accounting for both wall slip layer and particle heterogeneities resulting from shear-induced particle migration. The predicted flow field is then used to estimate the pressure-flow rate relationship and pipe wear rate, both critical factors in industrial operations. Experimental loop tests are conducted to examine the pressure drop–flow velocity relationship of CPB with varying solid concentrations. The developed numerical model is then validated using the loop test results and existing literature data. Subsequently, particulate flow dynamics in CPB pipelines are explored, and parametric studies are conducted to provide practical guidelines for optimising CPB delivery operations. The paper is outlined with five main sections. Sections 2 and 3 present details of numerical and experimental methods, respectively. In the numerical methods, an advanced CFD model is developed, which considers particle migration and wall slip to accurately predict flow behaviour, pressure drop, and pipe wear under various operating conditions. In the experimental methods, both rheology tests and loop tests are used to determine the rheological and flow behaviours of CPB mixtures. Section 4 validates the developed CFD models by comparing the numerical results to the experimental data obtained. A parametric study is conducted in Section 5 to correlate the key factors and flow behaviours for design optimisation. In Section 6, conclusions are drawn based on the research findings and outcomes.

2. Numerical Modelling Method

This section outlines the numerical framework developed to simulate CPB flow behaviour in pipelines. The model integrates fluid dynamics, particle migration, and wall slip effects to accurately predict flow behaviour, pressure drop, and pipe wear under various operating conditions.

2.1. Fluid Dynamics

In this numerical framework, the backfill is considered as a continuous suspension. Its fluid dynamic follows the continuity equation,

$$\nabla \cdot \mathbf{u} = 0, \tag{1}$$

and the momentum conservation equation,

$$\rho\left(\frac{\partial \mathbf{u}}{\partial t}+\mathbf{u}\cdot\nabla\mathbf{u}\right)=-\nabla p+\nabla\cdot\boldsymbol{\tau}+\rho\mathbf{g}, \tag{2}$$

where $\mathbf{u}$ is the fluid velocity, ρ is the fluid density, p is the pressure, $\boldsymbol{\tau}$ is the stress tensor, and $\mathbf{g}$ is the body force, respectively.

The Bingham model [27] is adopted to describe the flow behaviour of the backfill:

$$\begin{array}{ll}\boldsymbol{\tau}=2(\mu_P+\dfrac{\tau_0}{|\mathbf{D}|})\mathbf{D}, & |\boldsymbol{\tau}|\geq\tau_Y\\ \mathbf{D}=0, & |\boldsymbol{\tau}|<\tau_Y\end{array}, \tag{3}$$

where μ_p is the plastic viscosity, τ_Y is the yield stress threshold, τ_0 is the yield stress, $\boldsymbol{\tau}$ is the stress tensor, and $\mathbf{D}$ is the rate of deformation tensor, respectively. The shear rate $\dot{\gamma}$ can be represented as the magnitude of the rate of deformation tensor, $\dot{\gamma}=\sqrt{\frac{1}{2}(\mathbf{D}:\mathbf{D})}$.

Considering the inhomogeneous distribution of the particle concentration, the rheology of the suspension is described using the Krieger model [28]:

$$\mu=\mu_0(1-\frac{\phi}{\phi_m})^{-[\eta]\phi_m}, \tag{4}$$

where ϕ_m is the maximum packing density of the particles, μ_0 is the viscosity of the pure solvent (suspending medium), and $[\eta]$ is the intrinsic viscosity, which indicates how individual particles affect the viscosity of the suspension. The yield stress of CPB is related to the concentration of the solid particles by using the Chateau–Ovarlez–Trung model [29]:

$$\tau_Y=\tau_0\sqrt{\frac{1-\phi}{(1-\dfrac{\phi}{\phi_m})^{\,[\tau]\phi_m}}}, \tag{5}$$

where τ_0 is the yield stress of suspending fluid, and $[\tau]$ is the coefficient similar to intrinsic viscosity. Both the Krieger model and the Chateau–Ovarlez–Trung model have been widely applied to predict the viscosity and yield stress in suspensions with high particle concentrations.

2.2. Shear-Induced Particle Migration

The Diffusion Flux Model (DFM) predicts shear-induced particle migration in concentrated suspensions by describing particle motion due to diffusive fluxes driven by gradients in particle concentration, shear rate, and viscosity [22,30]. As a continuum-based modelling framework, it is particularly suitable for fine-particle slurry systems, where particle-resolved methods are computationally impractical [31]. The total particle flux $\mathbf{J}$ is expressed as the sum of contributions from particle collision-induced diffusion $\mathbf{J}_c$ and viscosity gradient induced diffusion $\mathbf{J}_\eta$, such that $\mathbf{J}=\mathbf{J}_c+\mathbf{J}_\eta$. The first term $\mathbf{J}_c$ accounts for particle motion due to concentration gradients, and the shear-induced flux arises from hydrodynamic interactions driven by shear rate gradients, and it can be given as follows:

$$\mathbf{J}_c=-K_c a^2\left(\phi^2\nabla\dot{\gamma}+\phi\dot{\gamma}\nabla\phi\right) \tag{6}$$

where a is the particle diameter and K_c is an empirical coefficient in the order of $O(1)$. The second term $\mathbf{J}_\eta$ represents the resistance on the particles due to the inhomogeneous distribution of viscosity, given as the following:

$$\mathbf{J}_\eta=-K_\eta a^2\dot{\gamma}\phi^2\frac{1}{\mu}\frac{d\mu}{d\phi}\nabla\phi \tag{7}$$

where K_η is the empirical coefficient like K_c. The Lagrangian derivative of the particle concentration is expressed as the divergence of the total flux:

$$\frac{D\phi}{Dt} = -\nabla \cdot \mathbf{J}. \tag{8}$$

This model provides a robust framework for predicting non-uniform particle distributions in flow fields and has been widely applied in processes such as extrusion, microfluidics, and suspension-based manufacturing [32,33]. It should be noted that the above model was first developed to predict the particle migration behaviour in a Newtonian fluid. While several studies extended its application to yield stress materials [26,34], further experimental justifications of the assumption are needed in future work.

2.3. Wall Slip Effect

In addition to the shear-induced particle migration, the wall effects also change the particle distribution, especially in the near wall area. The influence area is related to the particle size and particle concentration, and the thickness of the slip layer δ is expressed as the following [35]:

$$\frac{\delta}{D_p} = 1 - \frac{\phi_{bulk}}{\phi_m} \tag{9}$$

where ϕ_{bulk} is the cross-section-averaged solid concentration and D_p is the harmonic mean diameter of the suspended particles calculated from the particle size distribution (PSD) as follows:

$$D_p = \left(\sum_i \frac{f_i}{d_i} \right)^{-1} \tag{10}$$

where d_i and f_i denote the particle diameter and its corresponding volume fraction, respectively. The slip layer is assumed to be the binder fluid containing a few particles, which exhibit much higher flowability than the bulk suspension. Due to the low viscosity and yield stress of the slip layer, the local velocity increases abruptly over a limited distance from the wall. This so-called "apparent slip" phenomena can be simplified as a slip velocity v_s at the confining walls, which can be expressed as follows [36]:

$$v_s = \delta \frac{\tau_w}{\eta_{slip}} \tag{11}$$

where τ_w is the wall shear stress, and η_{slip} is the viscosity of the slip layer. Despite this simplification, it is important to distinguish the wall slip effect in CPB from the true slip phenomena, where the fluid physically slips at the boundary of a solid surface [37]. The slip velocity formulation adopted in Equation (11) corresponds to a Navier-type slip model. It has been used in both laboratory-scale and full-scale CPB pipeline studies and has been shown to provide reliable predictions without requiring recalibration when pipe diameter changes [7,38]. Therefore, the present formulation was considered suitable for application across different pipe scales.

2.4. Wear Prediction

The wear of the pipeline surface caused by particulate flow in the backfill delivery systems is a complex phenomenon. In laminar pipe flow, sliding abrasion is the primary mechanism of material loss, while particle impact erosion can be neglected due to the flow characteristics and particle behaviour. In this regime, fluid motion is smooth and orderly, causing particles to follow streamlines closely and slide along the pipe wall rather than impacting at high angles. Surface material removal is driven by the abrasive action of particles under shear flow conditions, with the abrasive wear rate $E_{abrasive}$ dependent on the wall shear stress, particle sliding velocity, and the mechanical properties of both the abrasive particles and the wearing surface [39]:

$$E_{abrasive} = \frac{V_s \tau_w \phi_w}{E_{sp}} \tag{12}$$

where τ_w is the wall shear stress, V_s is the sliding velocity of particles, ϕ_w is the particle concentration around the wall, and E_{sp} is the empirically determined specific energy of the material, representing its resistance to erosion.

2.5. Model Implementation for CPB Pipe Flow

For fully developed CPB flow in the pipeline, the momentum conservation and DFM equations in cylindrical coordinates are expressed as follows:

$$\frac{dp}{dz} - \frac{1}{r}\frac{d}{dr}(r\tau_{rz}) = 0, \tag{13}$$

and

$$\frac{\partial \phi}{\partial t} = \nabla \cdot \left\{ a^2 K_c \left(\phi^2 \frac{\partial \dot{\gamma}}{\partial r} + \phi \dot{\gamma} \frac{\partial \phi}{\partial r} \right) + a^2 K_\eta \dot{\gamma} \phi^2 \frac{1}{\mu} \frac{\partial \eta}{\partial \phi} \frac{\partial \phi}{\partial r} \right\}. \tag{14}$$

The particle flow is subjected to the boundary condition at the wall, the particle flux through the wall is zero, and the flow velocity at the wall equals the slip velocity:

$$\mathbf{J} \cdot \boldsymbol{n} = 0 \text{ and } u = v_s \text{ at } r = R. \tag{15}$$

The gradient of velocity is zero due to the symmetry:

$$\frac{du}{dr} = 0 \text{ at } r = 0. \tag{16}$$

To determine the slip velocity v_s using Equation (11), the slip layer is considered as the binder fluid, i.e., water, which has a viscosity $\eta_{slip} = 0.001$ Pa·s. At the initial state, the particle distribution is assumed to be homogenous across the pipe section, i.e.,

$$\phi = \phi_0 \text{ for } 0 \le r \le R \text{ at } t = 0 \text{ and } \frac{du}{dr} = 0 \text{ at } r = 0 \tag{17}$$

where ϕ_0 is the initial particle concentration. As shown in Figure 1, by discretising the pipe spatially in the radial direction, the integral form of Equation (14) at time step t can be written as follows:

$$\int_{r_{j-\frac{1}{2}}}^{r_{j+\frac{1}{2}}} \int_t^{t+\triangle t} \frac{\partial \phi}{\partial t} r dt dr = \int_{r_{j-\frac{1}{2}}}^{r_{j+\frac{1}{2}}} \int_t^{t+\triangle t} a^2 \frac{\partial}{\partial r} \left\{ r \left[K_c \left(\phi^2 \frac{\partial \dot{\gamma}}{\partial r} + \phi \dot{\gamma} \frac{\partial \phi}{\partial r} \right) \right] + K_\eta \dot{\gamma} \phi^2 \frac{1}{\mu} \frac{\partial \mu}{\partial r} \right\} r dt dr. \tag{18}$$

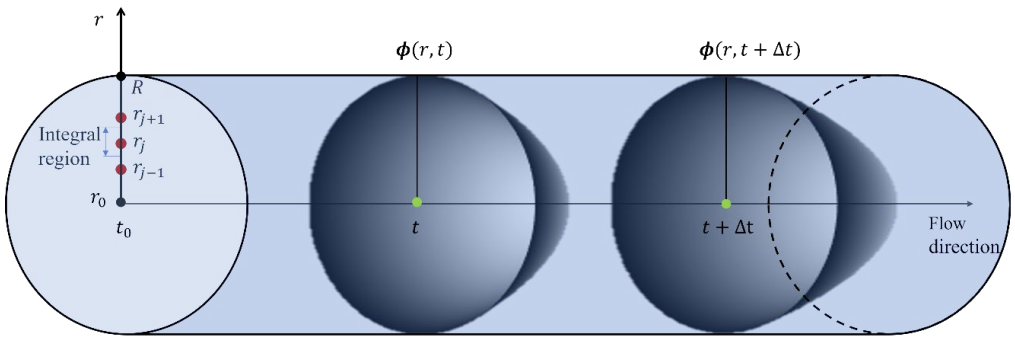


Figure 1. The schematic of the discretisation of the geometrical model of pipe flow, with the spatial and temporal distribution of the particle concentration profile.

Using a Crank–Nicolson finite difference scheme, Equation (18) can be finally written in the following form:

$$\mathbf{K}\phi^{t+\triangle t} = \mathbf{F} \tag{19}$$

where **K** and **F** are matrices related to the particle concentration profile at the last step ϕ^t, respectively. More information can be found in the literature [40].

Figure 2 provides an overview of the numerical framework. The model inputs include particle concentration, particle size, maximum particle packing density, rheological coefficients, and flow conditions such as flow velocity and pipe diameter. At each timestep, the spatial distributions of particle concentration, viscosity, and shear rate are updated iteratively until the fluxes $\mathbf{J}_c$ and $\mathbf{J}_\eta$ achieve equilibrium. Once particle migration reaches a steady state, the flow velocity profile is computed to generate the pressure-flow rate (P–Q) curve. Finally, the shear stress, particle velocity, and particle concentration at the wall are acquired to estimate the pipe wall abrasion rate based on Equation (12).

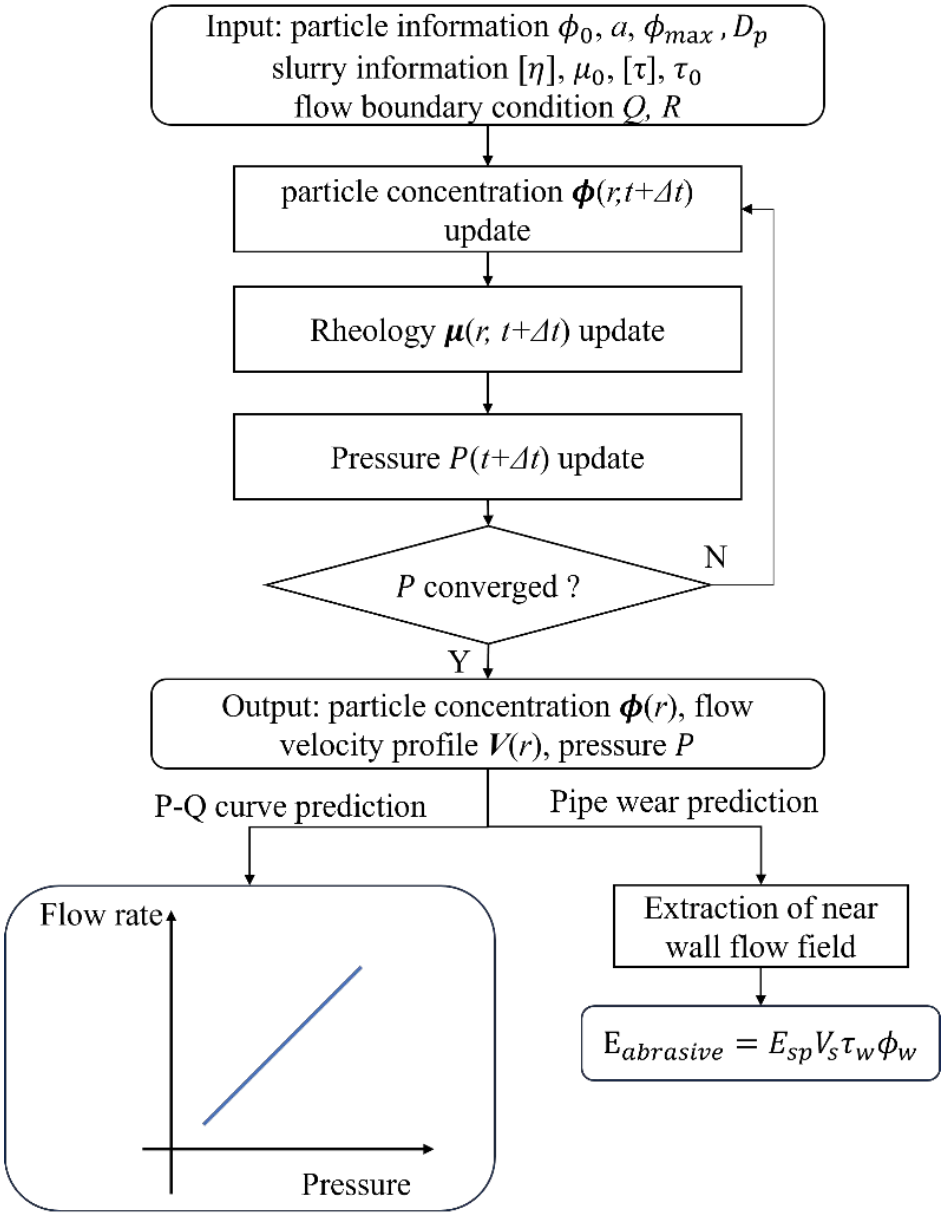


Figure 2. The flowchart for the numerical framework, including the input parameters, iteration algorithm, and outputs of the model.

3. Experimental Method

This section describes the experimental methods and setups used to investigate the rheological and flow behaviours of CPB. Rheology measurements and loop tests provide critical data for validating the numerical model and understanding the CPB rheology and pipeline flow dynamics.

3.1. Raw Materials and CPB Preparation

The tailings used in this work were sourced from a mining site in Australia, which are zinc tailings from the cyclone underflow of the flotation process. The solid specific gravity of the underflow tailings was measured to be 4.06 g/cm^3. The particle size distribution of the tailings is shown in Figure 3, characterised by D_{80} = 38 µm, D_{50} = 16.8 µm, and D_{20} = 5 µm, indicating a fine-grained material composition. The mean diameter and harmonic mean diameter were calculated to be 22.44 µm and 8.97 µm, respectively.

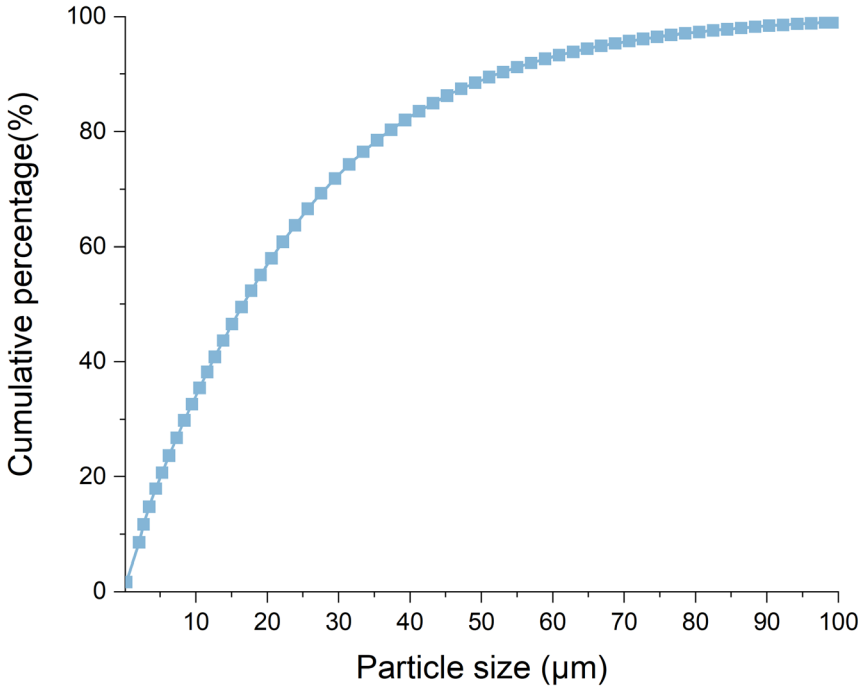


Figure 3. Particle sizing distribution for the underflow of Stockman zinc tailings.

CPB was prepared with solid contents of 66.3%, 74.8%, 77.6%, and 80.8%, corresponding to particle concentrations of 0.326, 0.422, 0.46, and 0.509, respectively. Solid contents above 80.8% were not considered, as the CPB becomes excessively stiff with very poor flowability, making stable pipeline transport impractical. In all cases, 4 wt.% of the total solid content was substituted with Ordinary Portland Cement (OPC) to serve as the binder addition.

3.2. Loop Test

The experimental loop test was conducted using a laboratory-scale pipeline with an internal diameter of 10.8 mm. The system consisted of a variable-speed metering pump, HDPE (high-density polyethylene) pipelines, and precision pressure transducers. The tailings were mixed with water to form an initial slurry for testing at the lower range of the designed solid contents. After each test, additional tailings were incrementally added to increase the solid contents up to 80.8%. Once loaded into the loop, the sample was pumped for five minutes to ensure homogeneous mixing. Pressure loss measurements were recorded for each sample at flow velocities ranging from 0.2 to 1.1 m/s,

providing data to analyse the relationship between pressure loss and the flow velocity for different slurries.

3.3. Rheology Test

In this study, the rheological properties of the CPB were evaluated using a Brookfield R/S+ Rheometer. The viscometer was operated at a controlled temperature of 28 °C. The shear procedure involved a pre-shear phase followed by a down-ramp phase. In the pre-share phase, the sample was subjected to a stepwise increase in shear rate, reaching 100 s^{-1} within 30 s, to disrupt particle agglomerates and ensure a homogeneous dispersion. After pre-shearing, in the down-ramp phase, the shear rate was gradually decreased from 100 s^{-1} to 0.1 s^{-1} over a period of 30 s. During the down-ramp phase, the torque required to rotate the vane was continuously measured, and the corresponding shear stress and shear rate were calculated. A linear regression was performed on the shear stress versus shear rate curve. The slope of the resulting line corresponds to the plastic viscosity, and the y-intercept represents the yield stress.

4. Validation of the Developed CFD Model

This section presents the measured critical rheological parameters, which serve as inputs for the model, and validate the numerical model by comparing the simulated results with experimental data and existing models. The validation process highlights the model's ability to capture complex rheological behaviour and flow dynamics of CPB, ensuring reliable pressure drop and wear rate estimations.

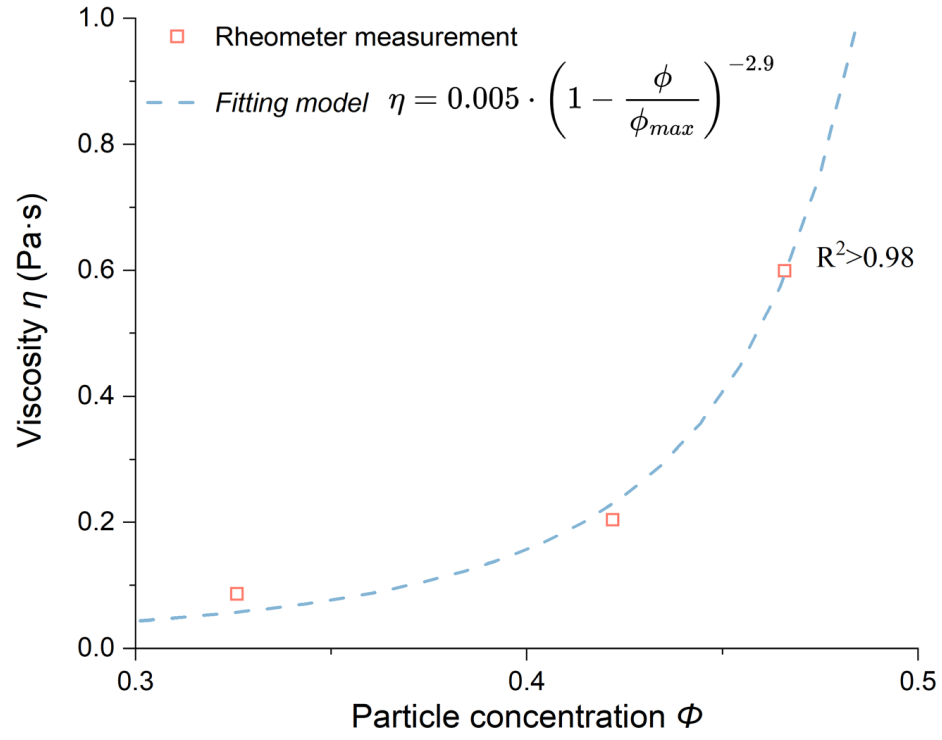
4.1. Determination of Input Rheological Parameters

The measured viscosity and yield stress of the slurry mixtures are presented in Figure 4a,b. The results focus on slurries with particle concentrations ranging from 0.326 to 0.46, as higher concentrations (i.e., 0.509) exceed the measurement capabilities of the rheometer. Both viscosity and yield stress exhibit significant increases with higher aggregate volume fractions. This trend is attributed to the higher probability of inter-particle collisions and interactions as particle concentration rises. These interactions promote the formation of particle clusters, which restrict fluid movement and increase the viscosity of the suspension.

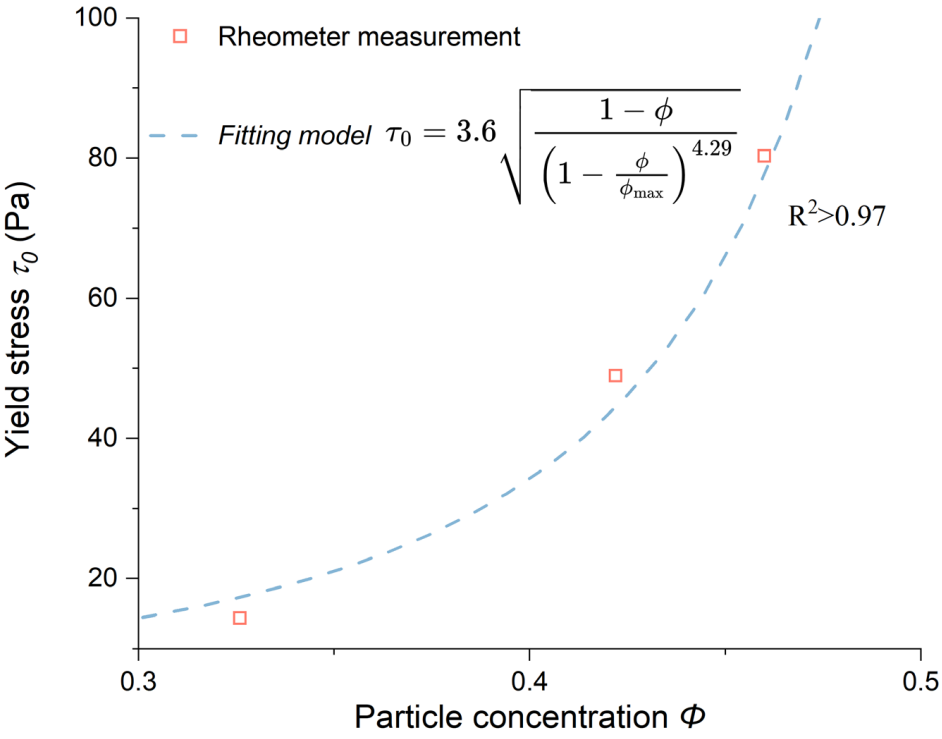
The viscosity and yield stress variations in CPB were analysed using two established rheological models: the Krieger model for viscosity and the Chateau–Ovarlez–Trung model for yield stress. The strong agreement between the experimental data and model predictions demonstrates these models' effectiveness in describing the relationship between particle concentration and the rheological behaviour of CPB. Despite the absence of one data point, the curve fitting reliably determines the critical parameters in Equation (4), which will serve as input for the numerical framework.

4.2. Mesh Convergence Test

A mesh sensitivity study was conducted to determine the optimal grid resolution for numerical simulations. The numerical simulation was configured based on the experimental setup materials used in the loop test, with a particle concentration of 46% and a flow velocity of 1 m/s. The fully developed velocity profile of the slurry flow was modelled using three different mesh configurations, varying the number of computational elements from 500 to 1500. As shown in Figure 5, the numerical velocity profiles for the three cases demonstrate close agreement, with the variation in the maximum velocity remaining below 0.2%. The pressure drop was also found to converge at 1000 intervals. Therefore, the mesh with 1000 intervals was adopted for all subsequent simulations.



(a)



(b)

Figure 4. (**a**) The measured viscosity of CPBs with different particle concentrations and fitting curve by the Krieger model, and (**b**) the measured yield stress of CPBs with different particle concentrations and fitting curve by the Chateau–Ovarlez–Trung model.

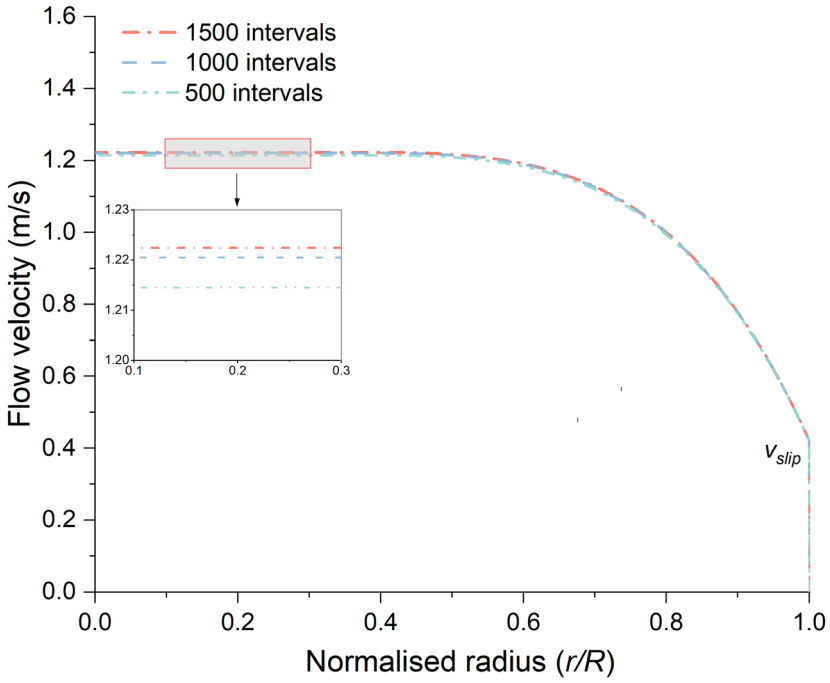


Figure 5. Velocity profiles of CPB flow with a particle concentration of 46% and a flow velocity of 1 m/s for CFD mesh resolutions ranging from 500 to 1500 intervals.

4.3. Pressure Prediction

Figure 6 illustrates the comparison between the experimental and numerical pressure drops of slurries at different flow velocities. The mean relative deviation was calculated by averaging the absolute percentage differences between experimental measurements and numerical predictions for each slurry, ranging from 7% to 17%. Notably, although the rheological parameters for the slurry with ϕ = 50.9% exceed the measurement limits of the viscometer, making them unavailable as direct model inputs, its pressure-velocity relationship was still captured with a high degree of accuracy. This is attributed to the incorporation of the Krieger model into the numerical framework, which allows reliable extrapolation of flow behaviours across a wide range of solid concentrations based on rheological measurements from a limited set of calibration cases. The accuracy of the pressure prediction can be further improved by incorporating additional experimental data at different solid concentrations to construct a more accurate rheological curve for the inputs of the numerical model.

To further evaluate the performance of the proposed model, it was compared with the wall slip model introduced in [7,38]. These two studies provide both full-scale experimental measurements and corresponding predictions obtained using a wall slip formulation. The experimental configurations adopted in the full-scale tests are summarised in Table 1. The wall slip model, developed based on the Buckingham model, incorporates a correction parameter associated with the properties of the slip layer. Figure 7a and Figure 7b illustrate the pressure predictions from different models, using iron tailings slurry data from Wang et al. [7] and cemented copper tailings slurry data from Liu [38], respectively. The prediction of the wall slip model, as shown in Figure 7, may differ from the numerical results in [7,38] due to variations in the estimation of slip layer thickness. While studies in [7,38] used the mean particle diameter in their calculations of Equation (9), this study employed the harmonic mean diameter, which follows the definition of the original formulation in [35].

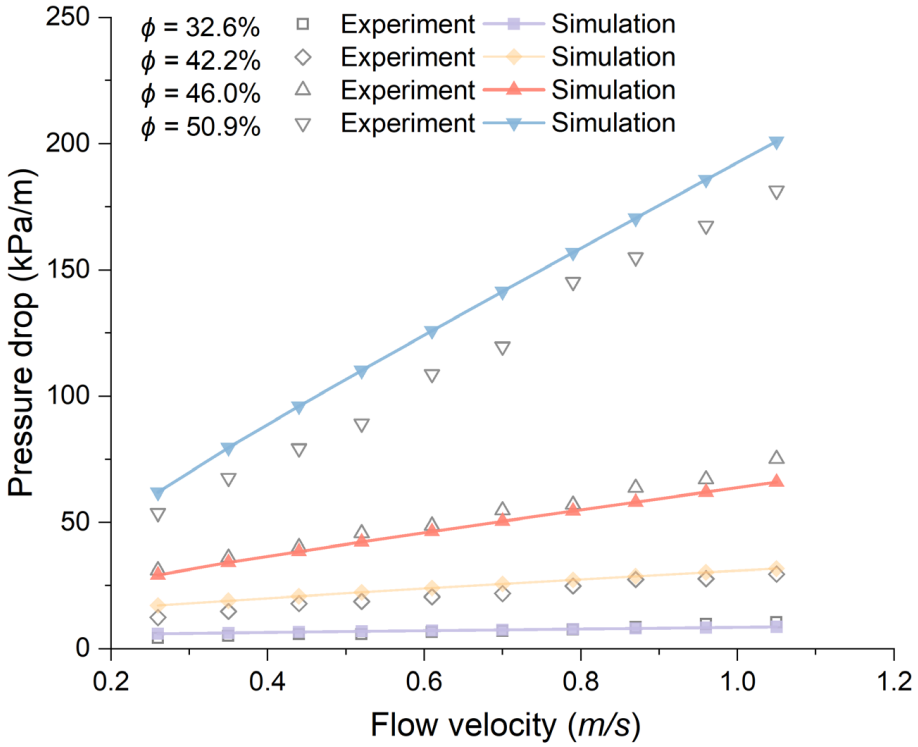


Figure 6. The comparison between the numerical and experimental pressure drops of slurries under different flow velocities.

Table 1. The experimental setup in the full-scale test from the literature [7,38].

Material	Pipe ID (mm)	Volume Fraction (%)	Velocity (m/s)
Iron Tailings Paste [7]	100	47.7, 50.3, 53.2	0.7–1.3
Cemented CopperTailings Paste [38]	150	46.2, 47.6, 48.8	0.4–1.0

The results demonstrate that the wall slip model tends to overpredict the pressure drop, indicating its limitation in fully capturing the flow behaviour of CPB pipelines. In contrast, the proposed model, which accounts for both wall slip and shear-induced particle heterogeneities, provides more accurate predictions when compared to experimental data. Compared to the wall slip model, the proposed model reduces the average prediction errors from 15% to 10% for iron tailings slurry [7] and from 24.3% to 5.3% for cemented copper tailings slurry [38]. This good agreement with the full-scale test confirms the applicability of the present model to industrial-scale CPB pipeline systems.

To ensure a consistent basis for comparison, the same wall slip parameters were used in both models to ensure a consistent basis for comparison, such that the observed improvement can be attributed to the inclusion of shear-induced particle migration. In the present study, a constant empirical value of $K_c/K_\eta = 0.66$ was adopted for all cases, which provides good agreement with the available experimental data. This ratio governs the extension of shear-induced particle migration, with larger values corresponding to more efficient migration and a greater reduction in pressure loss. While this value provided a reasonable representation for the CPB system considered here, slight variations in K_c/K_η may existed among different particulate suspensions due to differences in particle properties and interaction mechanisms. This parameter can be further refined for a specific material to improve the predictive accuracy of the devised numerical model.

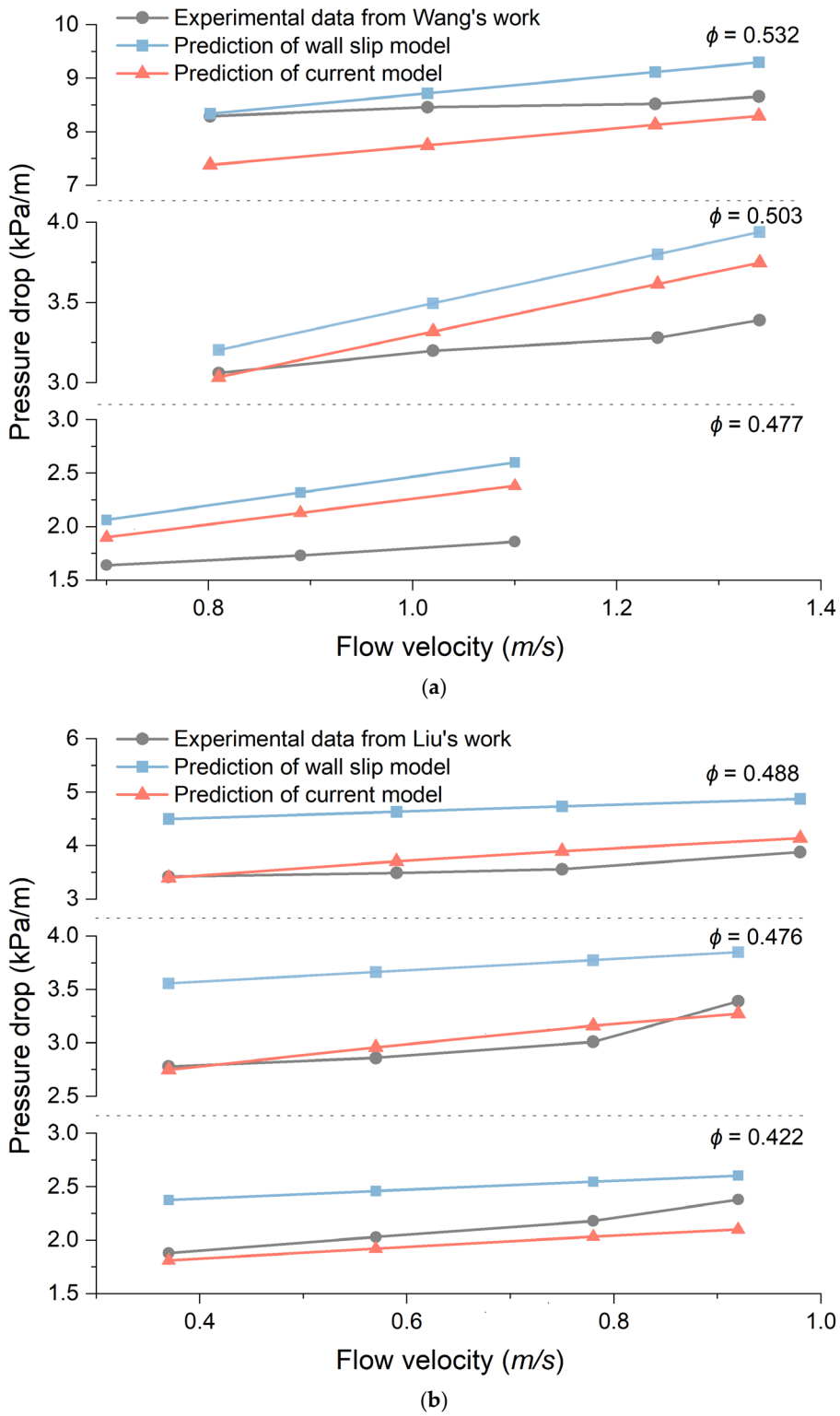


Figure 7. Comparison of experimental data with predictions using the current and the wall slip models for (**a**) iron tailings slurry [7] and (**b**) cemented copper tailings slurry [38].

4.4. Wear Prediction

The validation in Sections 4.2 and 4.3 demonstrates that the proposed model outperforms the existing model, providing a more reliable prediction of pressure drop in the pipeline. In this section, the accuracy of the model's wear prediction is validated against the experimental study conducted by Steward and Spearing [41], which investigates the

wear of steel pipelines under varying conditions of slurry relative density ρ_r, pipe diameter D, and flow velocity v. It is important to note that the rheological parameters were not provided in Steward's study [41]. Therefore, the input rheological parameters, such as $[\eta]$ and μ_0, were determined using an optimisation algorithm to best fit the experimental pressure–velocity relationship across all test scenarios in [41]. This approach is supported by the validated pressure predictions, which have been confirmed through loop test experiments and existing literature data. As shown in Equation (12), the key parameter in the wear model is the specific energy E_{sp}, which is strongly linked to material properties and wear conditions. Based on relevant studies on slurry erosion in steel pipes [42], E_{sp} is set to 2×10^{11} J/m^3.

Figure 8 presents a comparison between the experimental and numerical wear rates of the pipeline under different conditions of relative density, pipe diameter, and flow velocity. The results from [41] are presented in a unit of μm/t, representing micrometre loss per ton of solid mass flow through the pipe. For consistency with the unit of the $E_{abrasive}$ in Equation (12), these values are converted to units of m/s, which indicate the loss of meter thickness of the pipe wall per second of flow. The comparison reveals a strong agreement between experimental results and numerical predictions, except for a few cases with low relative density and high flow velocity. This deviation is attributed to the transition from laminar to turbulent flow in the pipe, which occurs at high velocity and low solid particle content. In turbulent flow, random particle impingement on the pipe wall becomes significant, exceeding the basic assumption of the model that particles slide along the wall. Despite the deviations observed in these specific cases, the prediction of wear rate by this model remains reliable.

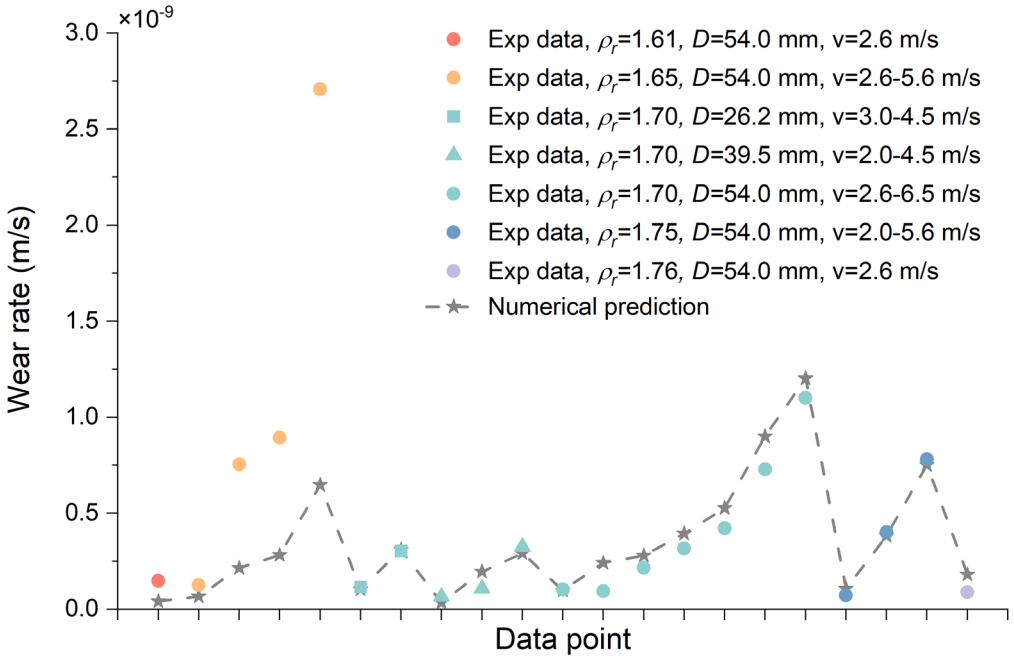


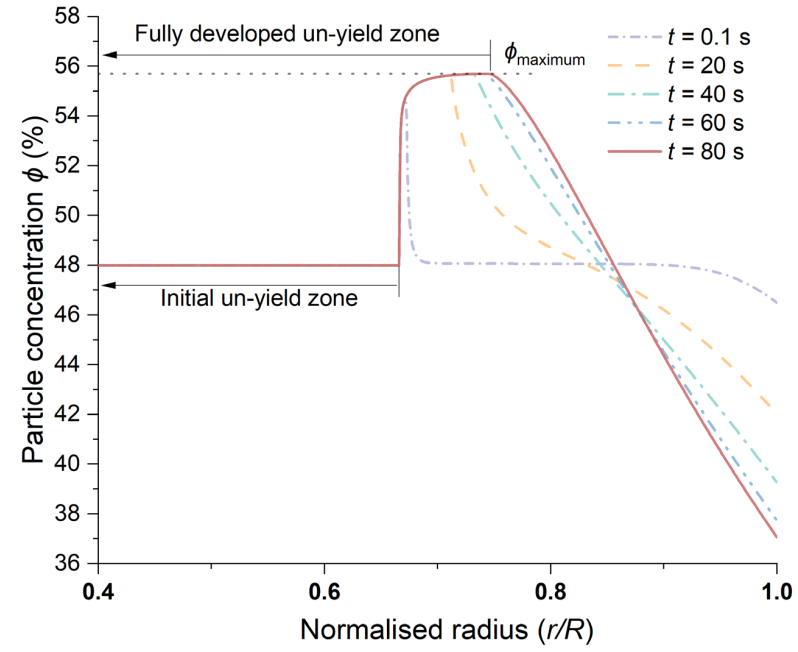
Figure 8. The comparison between the numerical wear rates and Steward's experimental results [41] for the pipeline under varying conditions of relative density, pipe diameter, and flow velocity.

5. Parametric Study

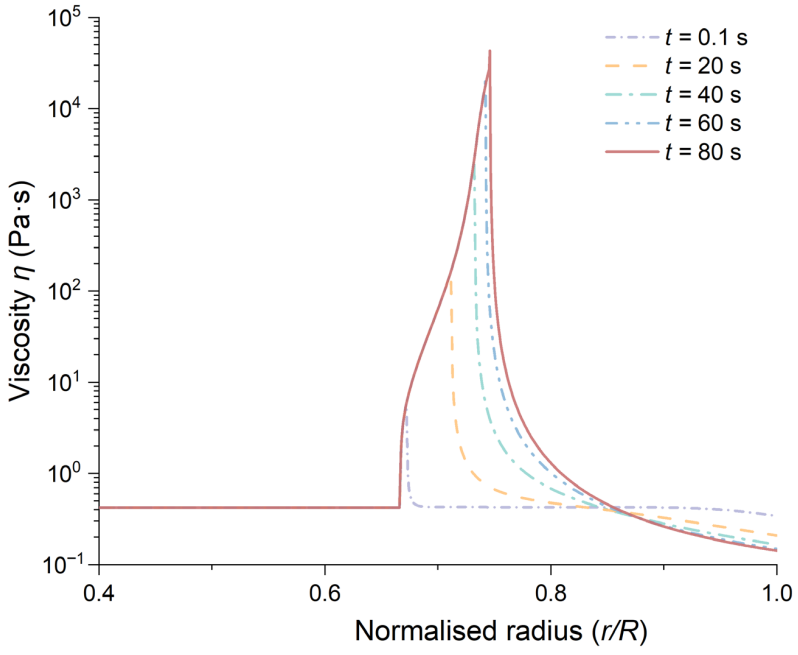
5.1. Flow Characteristics

After validating the model, a full-scale simulation of pipe flow was conducted to investigate how flow heterogeneities influence the dynamic behaviour of CPB in an industrial pipeline system. The pipe flow of CPB with a 48% solid particle concentration from Liu's

work [38] is analysed numerically based on the full-scale validation presented in Section 4.3. The modelled pipeline has a diameter of 150 mm and a flow velocity of 2 m/s. Figure 9a shows the evolution of the particle concentration profile along the pipe radius. Initially, the CPB enters the pipe as a homogeneous mixture, with a uniform particle concentration across the cross-section. As the flow develops, particles begin to migrate from the pipe wall toward the centre. However, due to the high yield stress of CPB, a plug flow forms near the pipe centre, where the material flows as an unyielded solid. This unyielded zone inhibits further particle migration, leading to particle accumulation at the boundary of the unyielded region.



(**a**)



(**b**)

Figure 9. The evolution of (**a**) particle concentration profiles and (**b**) viscosity profiles along the pipe radius with the flow time.

The local rheology of CPB is significantly affected by particle heterogeneities, as viscosity is strongly correlated with particle concentration. As shown in Figure 9b, the local viscosity near the pipe wall decreases, while the viscosity near the unyielded boundary increases. Given that the shear stress near the pipe wall is much higher than in the unyielded boundary region, this change in the viscosity profile reduces the pressure drop required to maintain the same flow rate. The reduced pressure drop then causes the unyielded zone to expand, as the radius of the unyielded zone is linearly related to the pressure drop. This explains the observed drift of the unyielded boundary toward the pipe wall on Figure 9a. As particle migration progresses, the particle concentration at the unyielded boundary gradually approaches the maximum packing density, ϕ_m. Once the flux driven by the shear gradient, J_c, balances with the flux caused by viscosity inhomogeneities, J_η, the system reaches a steady state. At this point, both the particle concentration and viscosity profiles stabilise, and no further changes in the flow behaviour are observed. A schematic of the particle migration process and evolution of the particle concentration and viscosity profile along the flow direction is given in Figure 10.

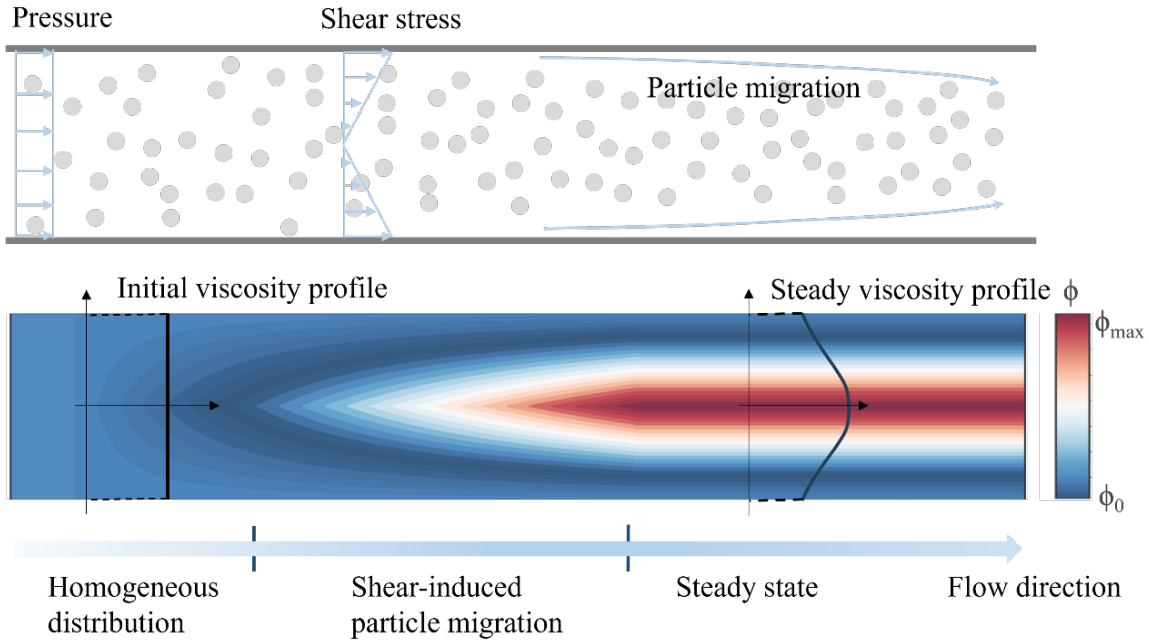
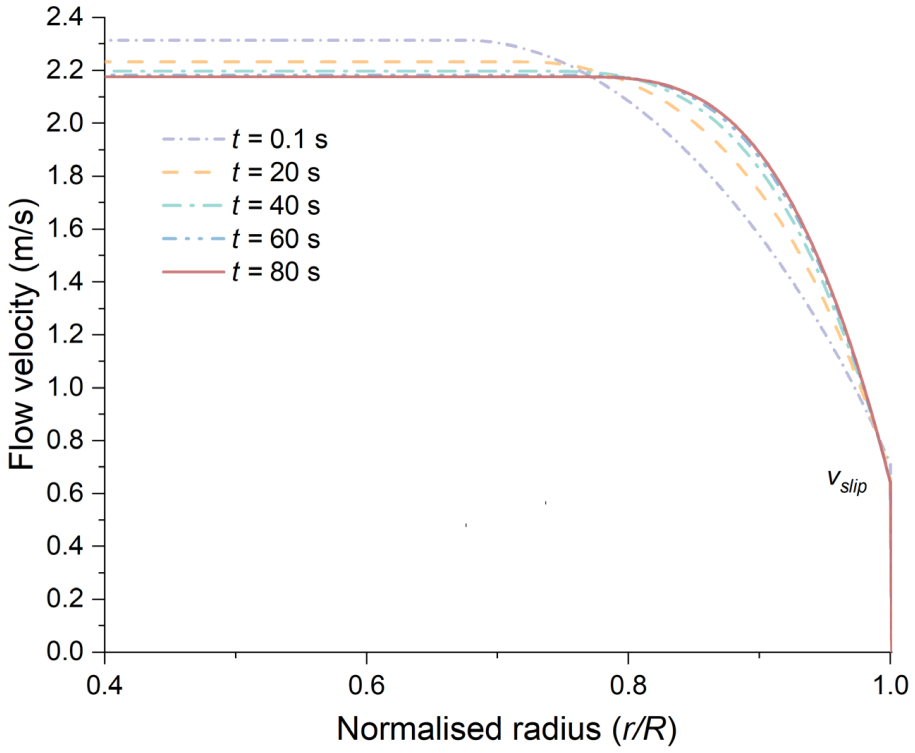
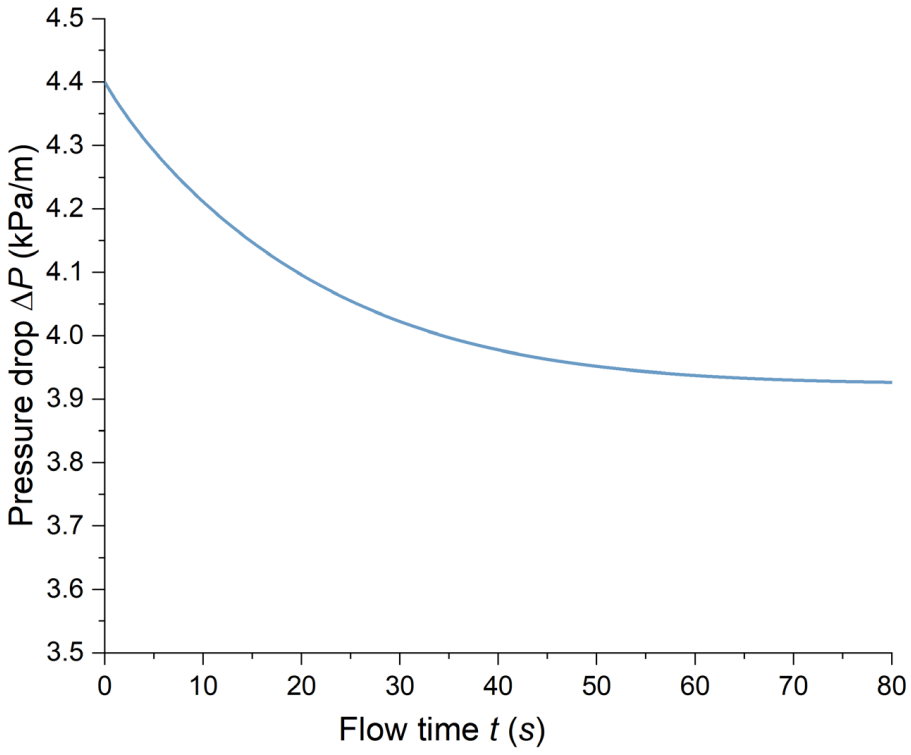


Figure 10. The schematic of the particle migration process and evolution of the particle concentration and viscosity profile along the flow direction (The contour and profile curves are illustrative and do not represent exact values).

Figure 11a and Figure 11b illustrate the evolution of the velocity profile and pressure gradient over time. As particle migration progresses, the velocity gradient near the boundary increases. Meanwhile, the maximum velocity within the pipe decreases due to the rise in local viscosity near the pipe centre. To satisfy the inlet boundary condition of a constant flow rate, the integral of the velocity profile, i.e., the area under the velocity curve across the pipe radius, remains unchanged. As local viscosity within the yielded zone decreases, the pressure gradient continues to drop to maintain this constant flow rate. This reduction in pressure gradient leads to an expansion of the unyielded zone. These observations align with findings from previous studies on Newtonian suspensions [43] and Bingham suspensions [34].



(**a**)



(**b**)

Figure 11. (**a**) Evolution of the velocity profile along the pipe radius over flow time, and (**b**) evolution of the pressure drop in the pipeline over flow time.

It is important to note that the above-mentioned analysis assumes an ideal, constant flow rate at the inlet. However, flow conditions in real backfill pipelines are far more complex, particularly in gravity-driven backfill operations. These complex bound-

ary conditions can significantly alter the velocity profile and pressure distribution along the pipeline.

5.2. Effects of Pipe Diameter, Flow Velocity, and Solid Concentration on Flow Behaviours

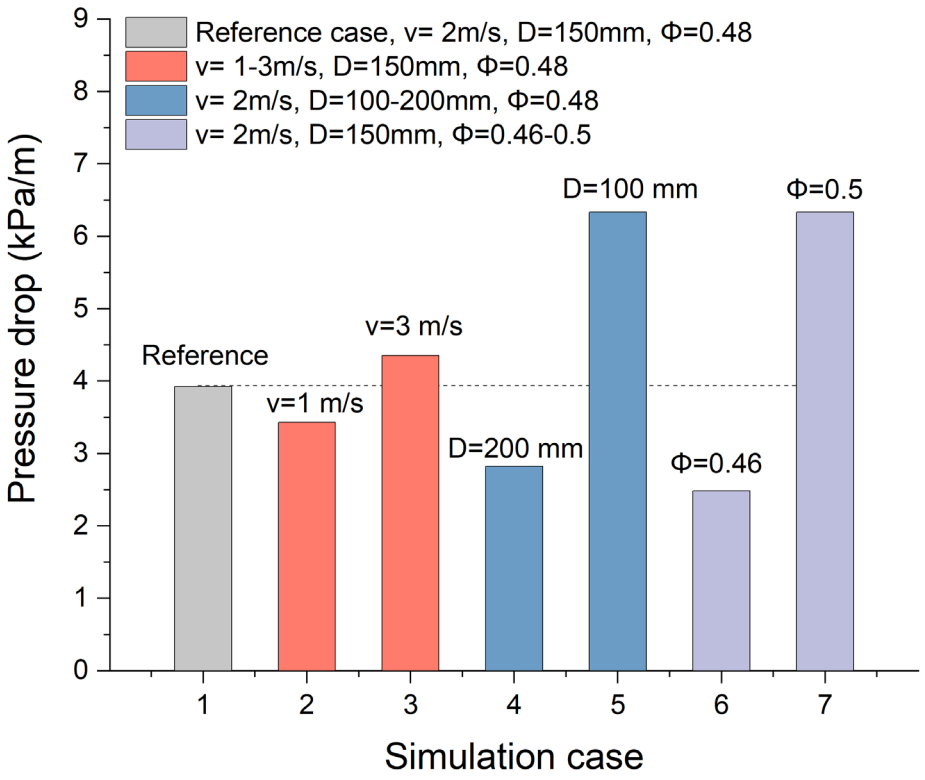
Based on the flow characteristics presented in the previous section, a parametric study was conducted to evaluate the effects of pipe diameter, flow velocity, and solid concentration on particulate flow behaviours. The simulations were performed for seven cases in total, as given in Table 2. Case 1, designated as the reference case, featured a pipe diameter of 150 mm, a flow velocity of 2 m/s, and a solid concentration of 48%. In Cases 2 and 3, the flow velocity was 1 m/s and 3 m/s, respectively, while maintaining the same pipe diameter and solid concentration as the reference. Cases 4 and 5 explored pipe diameters of 100 mm and 200 mm, while cases 6 and 7 adjusted solid concentration to 46% and 50%, respectively. This systematic approach facilitates a comprehensive understanding of the individual and combined influences of these parameters on flow dynamics.

Table 2. Simulation cases with varying pipe diameters, flow velocities, and solid concentrations.

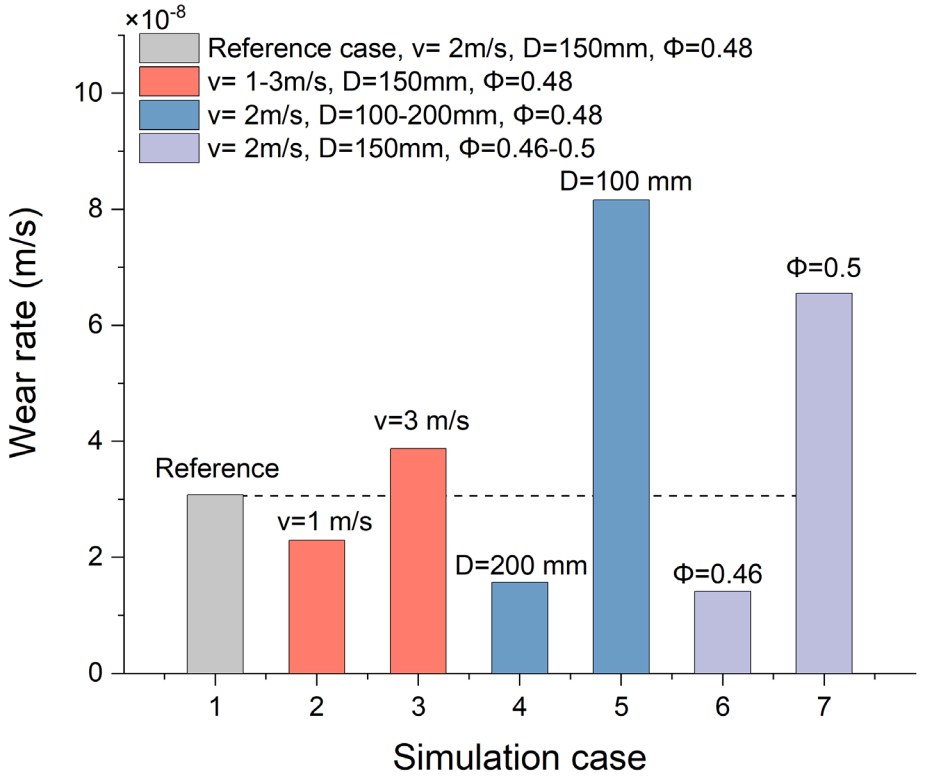
Simulation Case	Pipe Diameter D	Flow Velocity v	Solid Concentration Φ
1	150 mm	2 m/s	48%
2	150 mm	1 m/s	48%
3	150 mm	3 m/s	48%
4	100 mm	2 m/s	48%
5	200 mm	2 m/s	48%
6	150 mm	2 m/s	46%
7	150 mm	2 m/s	50%

Figure 12a illustrates the impacts of flow velocity, pipe diameter, and particle concentration on pressure drop in backfill pipeline systems. The results show that pressure drop increases with higher flow velocities. From v = 1 m/s to 2 m/s, the pressure drops increase by 0.495 kPa/m, and from 2 m/s to 3 m/s, it increases by 0.427 kPa/m. The results suggest a near-linear relationship between pressure drop and flow velocity, primarily governed by the viscosity of CPB. In Newtonian suspensions, the steady-state particle distribution due to shear-induced migration is independent of flow velocity. However, in dense slurries like those in this study, increased flow velocity can shrink the plug flow region, potentially altering particle distribution. While this could introduce some nonlinearity, the current findings indicate that its impact remains minimal.

The relationship between pipe diameter and pressure drop shows notable nonlinearity, with pressure drop increasing significantly as the pipe diameter decreases. In smaller pipes, the surface area in contact with the slurry increases relative to the flow cross-sectional area. This results in higher pressure losses due to intensified frictional interactions between the fluid and the pipe wall. Similarly, the relationship between particle concentration and pressure drop is nonlinear, as increasing particle concentration significantly alters the rheological properties of the mixture. This nonlinearity is governed by the power-law relationship between rheological parameters and particle concentration, as described in Equation (4).



(**a**)



(**b**)

Figure 12. Effects of flow velocity, pipe diameter, and particle concentration on (**a**) pressure drop and (**b**) wear rate. Note: The dashed line is drawn for easy comparison.

The numerical results of the pipe wear rate for all cases are given in Figure 12b. The wear rate of all cases remains at a relatively low level, i.e., in the order of 10^{-8} m/s, which

indicates the long-life service of the pipe under the laminar flow. For reference, the field measured wear rate of a pipeline in mine is around 2×10^{-8}–8×10^{-8} m/s (solid mass content 82%, flow velocity 2 m/s, 200 NB pipe) [44]. A higher wear rate is observed in cases with increased flow velocity and smaller pipe diameters, which aligns with findings in existing literature. Higher velocities result in more frequent and energetic particle-wall interaction, which intensifies abrasive wear. For smaller pipe diameters, the increased shear-rate gradient promotes shear-induced particle migration and tends to reduce the near-wall particle concentration [34]. However, the accompanying increase in wall shear stress and particle–wall interaction frequency dominates, leading to an overall increase in the erosion rate. Figure 12b illustrates that the increased solid concentration enhances the wear rate due to the intensified interaction between the slurry and the pipe wall. As shown in Figure 12a, dense slurries are associated with higher pressure drops, which correspond to increased wall shear stress. This increased stress, combined with a higher frequency of particle-wall interactions, accelerates abrasive wear on the pipe surface. Several studies have reported a decrease in pipe wear at higher solid concentrations, attributing this to the restricted motion of particles in dense suspensions [3]. When particle motion is constrained, the mean free path and impact energy are significantly reduced, leading to a transition in the dominant wear mechanism—from erosion, characterised by high-energy particle impacts, to abrasion, where particles slide along the pipe wall. This transition generally results in lower wear rates under such conditions. However, the current model focuses exclusively on abrasion wear in laminar flow conditions, without accounting for the complexities of erosive wear mechanisms or the effects of turbulence. Therefore, future work could expand the current model to incorporate these factors, providing a more comprehensive framework for predicting wear in diverse flow regimes and particle concentration ranges.

While this study investigates the individual impacts of v, D, and Φ, the superposition of these parameters in practical applications may induce synergistic effects. For instance, the combination of high velocity and high concentration is expected to exacerbate wear rates nonlinearly due to the coupled increase in particle impact frequency and kinetic energy. Similarly, the simultaneous occurrence of high concentration and reduced pipe diameter could lead to an exponential rise in pressure drop due to the non-Newtonian nature of the paste. Future studies using factorial design experiments could further quantify these cross-interaction effects.

6. Conclusions

An advanced CFD model was developed in this paper to predict the flow dynamics of the CPB in the paste reticulation circuit. Experimental studies, including rheometer test and loop test, were also conducted to validate the devised numerical modelling framework. It was found that the developed CFD model exhibits excellent capacities to predict the pressure drop as well as the pipe wear rate in the pipeline. The flow characteristics of the CPB were analysed in terms of the particle distribution and the evolution of the velocity profile and pressure. The parametric study was performed to investigate the effects of key determinants, such as pipe geometry, flow velocity and particle concentration. Based on these investigations, the conclusion can be drawn as follows:

- The prediction of pressure drops of the particle migration-based model outperforms the wall slip model. The prediction error is reduced from approximately 15% to 10% for uncemented tailings slurry, and from 24.3% to 5.3% for cemented tailings slurry.
- The prediction of pipe wear rate is in good agreement with the experimental measurement in loop tests. The wear rate of the pipeline for typical backfilling operations is determined to be in the range of 10^{-10} to 10^{-9} m/s, which is consistent with field measurements.

- Under constant flow conditions, particle migration from the pipe wall toward the unyielded boundary leads to heterogeneous particle distributions and spatially varying rheological properties. Elevated particle concentrations near the unyielded boundary increase the local viscosity to 10^{-5} Pa·s, thereby extending the unyielded zone. Conversely, the reduction in local viscosity near the pipe wall decreases flow resistance and reduces the overall pressure drop by up to 20%.
- Both the pressure drop and wear rate increase in the flow with denser solids, higher velocity and smaller pipe diameter. Compared to the velocity, the particle concentration and pipe diameter have a more pronounced or nonlinear effect on the pressure drop and wear rate.

The applicability of the present model is constrained by the assumptions of laminar flow and a simplified representation of wall slip, in which a uniform slip layer with the viscosity of the binder fluid is employed. While this treatment captures the dominant lubrication effect at the pipe wall, it does not explicitly resolve the gradual variation in particle concentration or the possible presence of fine particles within the slip layer, particularly under high solid concentrations or varying particle size distributions. Future work will focus on extending the model to account for high-velocity turbulent flow, more realistic near-wall particle dynamics, and time-dependent rheological behaviour. These developments are expected to enhance the robustness of the framework and broaden its applicability to a wider range of practical backfilling scenarios in industrial operations.

Author Contributions: Conceptualization, X.X., R.Y. and Y.X.Z.; methodology, X.X. and R.Y.; software, X.X.; validation, R.Y., Y.X.Z., K.D., Z.Z., S.C., D.H. and A.S.-G.; formal analysis, X.X.; investigation, X.X., R.Y., Y.X.Z. and S.C.; resources R.Y., Y.X.Z., K.D., Z.Z., S.C., D.H. and A.S.-G.; data curation, X.X.; writing—original draft preparation, X.X.; writing—review and editing, R.Y., Y.X.Z., K.D., Z.Z., S.C., D.H. and A.S.-G.; visualisation, X.X.; supervision, R.Y. and Y.X.Z.; project administration, R.Y.; funding acquisition, R.Y., Y.X.Z., K.D., Z.Z., S.C. and D.H. All authors have read and agreed to the published version of the manuscript.

Funding: This research was funded by the Australian Research Council (ARC) via ARC Linkage Project LP220100131: Transforming pastefill delivery system for next-generation mining industry and ARC Industrial Transformation Training Centres Funding Scheme—IC220100028: ARC Training Centre for Innovative Composites for the Future of Sustainable Mining Equipment.

Institutional Review Board Statement: Not applicable.

Informed Consent Statement: Not applicable.

Data Availability Statement: The data that support the findings of this study are available on request from the corresponding authors, Y.X.Z. and R.Y. The data are not publicly available due to their containing information that could compromise the privacy of our research participants.

Conflicts of Interest: Authors Scott Cheevers, Dean Harty and Andrew Stonier-Gibson were employed by the company Metrologi Pty Ltd. The remaining authors declare that the research was conducted in the absence of any commercial or financial relationships that could be construed as a potential conflict of interest.

References

1. Sivakugan, N.; Veenstra, R.; Naguleswaran, N. Underground Mine Backfilling in Australia Using Paste Fills and Hydraulic Fills. *Int. J. Geosynth. Ground Eng.* **2015**, *1*, 18. [CrossRef]
2. Veenstra, R.; Rosewall, A.; Rose, H. Throttling a cemented paste backfill underground distribution system. In Proceedings of the Paste 2023: 25th International Conference on Paste, Thickened and Filtered Tailings, Calgary, AB, Canada, 29 April–3 May 2023; University of Alberta and Australian Centre for Geomechanics: Edmonton, AB, Canada; Perth, Australia, 2023; pp. 726–742. [CrossRef]

3. Mcguinness, M.A. Wear Profile of the Kidd Mine Pastefill Distribution System. Master's Thesis, McGill University, Montreal, QC, Canada, 2013.
4. Wang, X.; Wang, H.; Wu, A.; Kang, G. Wear law of Q345 steel under the abrasion–corrosion synergistic effect of cemented paste backfill. *Constr. Build. Mater.* **2022**, *332*, 127283. [CrossRef]
5. Wang, K.; Li, C.; Wang, Z.; Lu, J.; Li, Y.; Wang, Y. Insights into the relationship between particulate flow characteristics and local erosion behaviour under waterjet: The role of particle-fluid-surface interaction. *Eng. Appl. Comput. Fluid Mech.* **2024**, *18*, 2409201. [CrossRef]
6. Manzar, M.A.; Shah, S.N. Particle Distribution and Erosion During the Flow of Newtonian and Non-Newtonian Slurries in Straight and Coiled Pipes. *Eng. Appl. Comput. Fluid Mech.* **2009**, *3*, 296–320. [CrossRef]
7. Wang, H.; Wang, X.; Wu, A.; Peng, Q. A wall slip pressure gradient model of unclassified tailings paste in pipe flow: Theoretical and loop test study. *J. Non-Newton. Fluid Mech.* **2021**, *298*, 104691. [CrossRef]
8. Bharathan, B.; McGuinness, M.; Kuhar, S.; Kermani, M.; Hassani, F.P.; Sasmito, A.P. Pressure loss and friction factor in non-Newtonian mine paste backfill: Modelling, loop test and mine field data. *Powder Technol.* **2019**, *344*, 443–453. [CrossRef]
9. Wang, X.; Guo, J.; Wu, A.; Wang, H.; Jiang, H. Pressure drop of cemented high-concentration backfill in pipe flow: Loop test, model comparison and numerical simulation. *Phys. Fluids* **2023**, *35*, 103107. [CrossRef]
10. Ahmed, H.M.; Bharathan, B.; Kermani, M.; Hassani, F.; Hefni, M.A.; Ahmed, H.A.M.; Hassan, G.S.A.; Moustafa, E.B.; Saleem, H.A.; Sasmito, A.P. Evaluation of Rheology Measurements Techniques for Pressure Loss in Mine Paste Backfill Transportation. *Minerals* **2022**, *12*, 678. [CrossRef]
11. Wu, A.; Ruan, Z.; Shao, Y.; Wang, J.; Yin, S.; Wang, S.; Li, C. Friction losses of cemented unclassified iron tailings slurry based on full-scale pipe-loop test. In Proceedings of the 22nd International Conference on Paste, Thickened and Filtered Tailings, Cape Town, South Africa, 6–10 May 2019; Australian Centre for Geomechanics: Perth, Australia, 2019; pp. 571–578. [CrossRef]
12. Dong, H.; Aziz, N.A.; Shafri, H.Z.M.; Ahmad, K.A.B. Computational fluid dynamics study on cemented paste backfill slurry: Review. *Constr. Build. Mater.* **2023**, *369*, 130558. [CrossRef]
13. Wang, L.; Cheng, L.; Yin, S.; Yan, Z.; Zhang, X. Multiphase slurry flow regimes and its pipeline transportation of underground backfill in metal mine: Mini review. *Constr. Build. Mater.* **2023**, *402*, 133014. [CrossRef]
14. Singalreddy, S.P.; Cui, L.; Fang, K. Spatiotemporal evolution of thermo-hydro-mechanical-chemical processes in cemented paste backfill under interfacial loading. *Int. J. Min. Sci. Technol.* **2022**, *32*, 1207–1217. [CrossRef]
15. Ghirian, A.; Fall, M. Strength evolution and deformation behaviour of cemented paste backfill at early ages: Effect of curing stress, filling strategy and drainage. *Int. J. Min. Sci. Technol.* **2016**, *26*, 809–817. [CrossRef]
16. Wu, A.; Ruan, Z.; Wang, J. Rheological behavior of paste in metal mines. *Int. J. Miner. Met. Mater.* **2022**, *29*, 717–726. [CrossRef]
17. Guo, Z.; Qiu, J.; Pel, L.; Zhao, Y.; Zhu, Q.; Kwek, J.W.; Zhang, L.; Jiang, H.; Yang, J.; Qu, Z. A contribution to understanding the rheological measurement, yielding mechanism and structural evolution of fresh cemented paste backfill. *Cem. Concr. Compos.* **2023**, *143*, 105221. [CrossRef]
18. Zhao, Y.; Taheri, A.; Karakus, M.; Chen, Z.; Deng, A. Effects of water content, water type and temperature on the rheological behaviour of slag-cement and fly ash-cement paste backfill. *Int. J. Min. Sci. Technol.* **2020**, *30*, 271–278. [CrossRef]
19. Zhang, L.; Wang, H.; Wu, A.; Klein, B.; Zhang, X. A constitutive model for thixotropic cemented tailings backfill pastes. *J. Non-Newton. Fluid Mech.* **2021**, *295*, 104548. [CrossRef]
20. Cheng, H.; Wu, S.; Li, H.; Zhang, X. Influence of time and temperature on rheology and flow performance of cemented paste backfill. *Constr. Build. Mater.* **2020**, *231*, 117117. [CrossRef]
21. Krishnan, G.P.; Beimfohr, S.; Leighton, D.T. Shear-induced radial segregation in bidisperse suspensions. *J. Fluid Mech.* **1996**, *321*, 371–393. [CrossRef]
22. Leighton, D.; Acrivos, A. The Shear-Induced Migration of Particles in Concentrated Suspensions. *J. Fluid Mech.* **1987**, *181*, 415–439. [CrossRef]
23. Xie, X.; Liu, X.; Zhang, L. New insight on particle migration of concrete under pumping based on X-ray computed tomography. *Cem. Concr. Compos.* **2024**, *149*, 105492. [CrossRef]
24. Xue, Z.; Sun, H.; Gan, D.; Yan, Z.; Liu, Z. Wall slip behavior of cemented paste backfill slurry during pipeline based on noncontact experimental detection. *Int. J. Miner. Met. Mater.* **2023**, *30*, 1515–1523. [CrossRef]
25. Yan, Z.; Yin, S.; Chen, X.; Wang, L. Rheological properties and wall-slip behavior of cemented tailing-waste rock backfill (CTWB) paste. *Constr. Build. Mater.* **2022**, *324*, 126723. [CrossRef]
26. Xie, X.; Zhang, L.; Shi, C.; Liu, X. Prediction of lubrication layer properties of pumped concrete based on flow induced particle migration. *Constr. Build. Mater.* **2022**, *322*, 126115. [CrossRef]
27. Bingham, E.C. *Fluidity and Plasticity*; McGraw-Hill Book Company, Incorporated: New York, NY, USA, 1922.
28. Krieger, I.M.; Dougherty, T.J. A mechanism for non-Newtonian flow in suspensions of rigid spheres. *Trans. Soc. Rheol.* **1959**, *3*, 137–152. [CrossRef]

29. Chateau, X.; Ovarlez, G.; Trung, K.L. Homogenization approach to the behavior of suspensions of noncolloidal particles in yield stress fluids. *J. Rheol.* **2008**, *52*, 489–506. [CrossRef]
30. Phillips, R.J.; Armstrong, R.C.; Brown, R.A.; Graham, A.L.; Abbott, J.R. A constitutive equation for concentrated suspensions that accounts for shear-induced particle migration. *Phys. Fluids A Fluid Dyn.* **1992**, *4*, 30–40. [CrossRef]
31. Zhou, H.; Wang, G.; Jia, C.; Li, C.; Novel, A. Coupled CFD-DEM Model for the Flow Characteristics of Particles Inside a Pipe. *Water* **2019**, *11*, 2381. [CrossRef]
32. Fataei, S.; Secrieru, E.; Mechtcherine, V.; Roussel, N. A first-order physical model for the prediction of shear-induced particle migration and lubricating layer formation during concrete pumping. *Cem. Concr. Res.* **2021**, *147*, 106530. [CrossRef]
33. Shauly, A.; Wachs, A.; Nir, A. Shear-induced particle migration in a polydisperse concentrated suspension. *J. Rheol.* **1998**, *42*, 1329–1348. [CrossRef]
34. Lavrenteva, O.M.; Nir, A. Shear-induced particles migration in a Bingham fluid. *J. Non-Newton. Fluid Mech.* **2016**, *238*, 80–91. [CrossRef]
35. Kalyon, D.M. Apparent slip and viscoplasticity of concentrated suspensions. *J. Rheol.* **2005**, *49*, 621–640. [CrossRef]
36. Mooney, M. Explicit formulas for slip and fluidity. *J. Rheol.* **1931**, *2*, 210–222. [CrossRef]
37. Cloitre, M.; Bonnecaze, R.T. A review on wall slip in high solid dispersions. *Rheol. Acta* **2017**, *56*, 283–305. [CrossRef]
38. Li, H. Study on Rheological Behavior and Pipe Flow Resistance of Paste Backfill. Ph.D. Thesis, University of Science and Technology Beijing, Beijing, China, 2015.
39. Krishna, R.; Kumar, N.; Gupta, P.K. Numerical study of wall erosion using energy approach for the flow of dense slurry in 90o horizontal pipe bend. *Powder Technol.* **2023**, *426*, 118623. [CrossRef]
40. Patankar, S.V. *Numerical Heat Transfer and Fluid Flow*; CRC Press: Boca Raton, FL, USA, 2018. [CrossRef]
41. Steward, N.R.; Spearingt, A.S. The performance of backfill pipelines. *J. S. Afr. Inst. Min. Metal.* **1992**, *92*, 27–34.
42. Clark, H.M.; Tuzson, J.; Wong, K.K. Measurements of specific energies for erosive wear using a Coriolis erosion tester. *Wear* **2000**, *241*, 1–9. [CrossRef]
43. Seifu, B.; Nir, A.; Semiat, R. Viscous dissipation rate in concentrated suspensions. *Phys. Fluids* **1994**, *6*, 3189–3191. [CrossRef]
44. Bharathan, B. Study of Wear and Viscous Heating in Paste Backfill Pipeline System. Master's Thesis, McGill University, Montreal, QC, Canada, 2016.

Disclaimer/Publisher's Note: The statements, opinions and data contained in all publications are solely those of the individual author(s) and contributor(s) and not of MDPI and/or the editor(s). MDPI and/or the editor(s) disclaim responsibility for any injury to people or property resulting from any ideas, methods, instructions or products referred to in the content.